

Cite as: A. Dutt *et al.*, *Science*
10.1126/science.aaz3071 (2019).

A single photonic cavity with two independent physical synthetic dimensions

Avik Dutt¹, Qian Lin², Luqi Yuan^{3*}, Momchil Minkov¹, Meng Xiao⁴, Shanhui Fan^{1*}

¹Ginzton Laboratory and Department of Electrical Engineering, Stanford University, Stanford, CA 94305, USA. ²Department of Applied Physics, Stanford University, Stanford, CA 94305, USA. ³State Key Laboratory of Advanced Optical Communication Systems and Networks, School of Physics and Astronomy, Shanghai Jiao Tong University, Shanghai 200240, China. ⁴Key Laboratory of Artificial Micro- and Nano-structures of Ministry of Education and School of Physics and Technology, Wuhan University, Wuhan 430072, China.

*Corresponding author. Email: yuanluqi@sjtu.edu.cn (L.Y.); shanhui@stanford.edu (S.F.)

The concept of synthetic dimensions has generated interest in many branches of science ranging from ultracold-atomic physics to photonics, as it provides a versatile platform for realizing effective gauge potentials and topological physics. Previous experiments have augmented the real-space dimensionality by one additional physical synthetic dimension. We endow a single ring resonator with two independent physical synthetic dimensions. Our system consists of a temporally modulated ring resonator with spatial coupling between the clockwise and counterclockwise modes, creating a synthetic Hall ladder along the frequency and pseudospin degrees of freedom for photons propagating in the ring. We observe a wide variety of rich physics, including effective spin-orbit coupling, magnetic fields, spin-momentum locking, a Meissner-to-vortex phase transition, and signatures of topological chiral one-way edge currents, completely in synthetic dimensions. Our experiments demonstrate that higher-dimensional physics can be studied in simple systems by leveraging the concept of multiple simultaneous synthetic dimensions.

There has been interest in creating synthetic dimensions to study classical and quantum dynamics (1) in systems with extra dimensions beyond their real-space geometric dimensionality (2). Synthetic dimensions can be formed by coupling atomic or photonic states with different internal degrees of freedom to form a lattice. These degrees of freedom could be based on the frequency, spin, linear momentum, orbital angular momentum, spatial supermodes or arrival time of light pulses (3). Previous experiments have provided demonstrations of $(d + 1)$ -dimensional physics on d -dimensional real-space lattices by using one extra synthetic dimension, for $d = 1$ (4, 5) or $d = 0$ (6–8). While theoretical proposals exist for creating two or more separate synthetic dimensions (9, 10), such proposals have eluded experimental observation so far. The realization of two or more synthetic dimensions drastically simplifies the experimental requirements for studying a rich set of topologically nontrivial phenomena, e.g., the high-dimensional quantum Hall effect (11, 12), without needing complex higher-dimensional structures in real space.

We demonstrate a system exhibiting two independent physical synthetic dimensions. Our system (Fig. 1A) consists of a ring resonator supporting a synthetic frequency dimension formed by the longitudinal cavity modes, and a synthetic pseudospin dimension formed by the clockwise (CW, \uparrow) and counterclockwise (CCW, \downarrow) modes at the same frequency. The coupling along the frequency dimension is achieved with a modulator (13). The coupling along the pseudospin dimension is achieved with an 8-shaped coupler, consisting of two

directional couplers connected by two nonintersecting waveguides. Our construction is different from methods of probing higher-dimensional phenomena using topological pumps, for which the physics with two extra dimensions has been explored in recent experiments (11, 12). In these systems, a mathematical mapping between higher-dimensional lattices and lower-dimensional systems is achieved by varying some external parameters of the lower-dimensional system (2, 14). Although signatures of higher-dimensional physics can be observed in such topological pumping schemes, the full dynamics are not captured because the external parameters are in fact not the dynamical variables of the particles (3). In contrast, our approach provides the ability to explore physical dynamics in higher dimensional space.

The tight-binding Hamiltonian describing our system is

$$H = -\sum_{m,s} \left[\omega_m a_{m,s}^\dagger a_{m,s} + \sum_{m'} J_{mm'}(t) a_{m,s}^\dagger a_{m',s} \right] - \sum_m K a_{m,\uparrow}^\dagger a_{m,\downarrow} e^{im\phi_0} + \text{H.c.} \quad (1)$$

where $a_{m,s}$ is the annihilation operator for the m -th longitudinal cavity mode with frequency $\omega_m = m\Omega_R$ and with pseudospin $s \in \{\downarrow, \uparrow\}$. $J_{mm'}(t)$ is the coupling along the synthetic frequency dimension (6, 13, 15, 16), produced by the electro-optic modulation (7). Due to a small portion of the ring being modulated, this coupling can be simplified as $J_{mm'}(t) = J \cos \Omega_R t$, i.e., the mode m can couple to all the other

modes of the system, and the coupling strength is independent of the mode indices (7). Here Ω_R is the free spectral range (FSR), corresponding to the separation between the longitudinal modes. K in Eq. 1 is the strength of the coupling between the two legs of the ladder, created by the 8-shaped coupler comprising two directional couplers with splitting amplitude \sqrt{K} . This coupling has a frequency-dependent and direction-dependent phase $\pm m\phi_0$ (Fig. 1B), with $\phi_0 \sim \pi \Delta L / L_0$ (17), where ΔL is the length difference between the two connecting waveguides, and L_0 is the length of the ring. To explain how this phase $\pm m\phi_0$ is introduced, we note that the connecting waveguide depicted by the blue solid line in Fig. 1A couples exclusively from the CW to the CCW mode, whereas the connecting waveguide depicted by the dashed line couples only from the CCW to the CW mode. The phase difference between the coupling in the two directions is therefore $\Delta\phi(\omega) = \phi_{\downarrow \rightarrow \uparrow} - \phi_{\uparrow \rightarrow \downarrow} = \beta(\omega)\Delta L$, where $\beta(\omega)$ is the propagation constant at frequency ω for a mode in the connecting waveguides. Assuming that the connecting waveguides are the same as the waveguide of the ring, and since $\beta(\omega_m) = 2\pi m / L_0$, the phase difference $\Delta\phi$ increases linearly with m : $\Delta\phi(\omega_m) = 2\pi m \Delta L / L_0 = 2m\phi_0$.

To transform Eq. 1 into a time-independent Hamiltonian, we define $b_{m,\uparrow} = a_{m,\uparrow} e^{-im(\Omega_R t + \phi_0/2)}$, and $b_{m,\downarrow} = a_{m,\downarrow} e^{-im(\Omega_R t - \phi_0/2)}$, and use the rotating-wave approximation to get

$$H = -\frac{J}{2} \sum_m (b_{m+1,\downarrow}^\dagger b_{m,\downarrow} e^{i\phi_0/2} + b_{m+1,\uparrow}^\dagger b_{m,\uparrow} e^{-i\phi_0/2}) - K \sum_m b_{m,\uparrow}^\dagger b_{m,\downarrow} + \text{H.c.} \quad (2)$$

This Hamiltonian describes a two-legged ladder pierced by a uniform magnetic field (a Hall ladder) (18), as each plaquette is threaded by an effective magnetic flux ϕ_0 (see Fig. 1, B and C). Thus, by choosing a nonzero ΔL , our structure in Fig. 1A naturally implements an effective magnetic field. Large magnetic fluxes spanning the entire range in $[-\pi, \pi]$ are achievable by choosing appropriate $\Delta L / L_0$. Since a purely 1D lattice does not permit magnetic field effects, our system corresponds to the simplest lattice model where the physics emerging from effective magnetic fields for photons can be observed.

Instead of describing the system in Fig. 1 as a two-legged ladder threaded by a uniform magnetic field, the physics of this system can alternatively be derived in terms of magnetic-field controlled spin-orbit coupling (SOC), with the CW and CCW modes of each ring representing up and down spins. Going to the quasimomentum space (k -space), the Hamiltonian in Eq. 2 becomes $H = \int dk \mathbf{b}_k^\dagger \mathcal{H}(k) \mathbf{b}_k$,

with $\mathbf{b}_k = \sqrt{\Omega / 2\pi} \sum_m e^{im\Omega k} (b_{m,\uparrow}, b_{m,\downarrow})^T$, and

$$\mathcal{H}(k) = -J \left[\mathbf{1}_2 \cos k\Omega \cos \frac{\phi_0}{2} + \sigma_z \sin k\Omega \sin \frac{\phi_0}{2} \right] - K \sigma_x \quad (3)$$

Here $\sigma_{x,y,z}$ are Pauli matrices. To make the SOC explicit, we recast Eq. 3 into the form, $\mathcal{H}(k) = \epsilon(k) \cdot \mathbf{1} + \mathbf{B}_{\text{SOC}}(k) \cdot \boldsymbol{\sigma}$, where $\epsilon(k) = J \cos k\Omega \cos(\phi_0/2)$, $\mathbf{B}_{\text{SOC}} = (K, 0, J \sin k\Omega \sin(\phi_0/2))$, and $\boldsymbol{\sigma} = (\sigma_x, \sigma_y, \sigma_z)$. The z -component of \mathbf{B}_{SOC} depends on the quasimomentum k , signifying spin-orbit coupling. The degree of SOC is controlled by the effective magnetic flux ϕ_0 . With the control of the magnetic flux, therefore, our system can exhibit a rich set of physics. Here we provide three experimental observations of such physics, all controlled by the magnetic gauge potential: spin-momentum locking in the band structure, chiral currents, and a Meissner-to-vortex phase transition.

The Hall ladder has been formally shown to exactly reproduce the energies and eigenstates of the topological chiral edge modes of a 2D quantum Hall insulator (Fig. 2A) described by the Hofstadter model (19). Even if the entire bulk lattice sites are removed, the strip of plaquettes forming the ladder retains the chiral currents and spin-momentum locking, as can be seen by comparing Fig. 2B to Fig. 2A. This attests to the topological robustness of the 2D quantum Hall insulator. Such signatures of topological chiral edge modes are evident in the theoretically calculated band structure of $\mathcal{H}(k)$ (Fig. 2, D and G) along with the corresponding color-coded pseudospin projections $n_\uparrow = \cos^2(\theta_B/2)$, $n_\downarrow = \sin^2(\theta_B/2)$ respectively. Here $\theta_B = \arctan[K/(J \sin k\Omega \sin(\phi_0/2))]$ represents the chiral Bloch angle of the eigenstate, and its k -dependence signifies chiral spin-momentum locking (19, 20): in the lower band, positive- (negative)- k states have predominantly CW (CCW) pseudospin character.

To directly detect the chiral modes of the Hall ladder, we use time-resolved band structure spectroscopy (7). We can selectively excite the CW or CCW pseudospin by exciting the waveguide from the left or right respectively, and measure the transmitted signal to map out the band structure projected onto the corresponding spin (17). The results of these measurements (Fig. 2, E and H) were obtained using a setup consisting of a fiber ring with an embedded electro-optic modulator and an 8-shaped coupler. The modulator is driven at $\Omega = 2\Omega_R = 29.6$ MHz (see (17) and (21) for details on the setup). The measured band structure agrees with that from the tight-binding model (Fig. 2, D and G), and also with simulations using a rigorous Floquet analysis (Fig. 2, F and I) (17). This constitutes a measurement of the dispersion of

chiral one-way states in synthetic dimensions. It is analogous to direct methods of interrogating surface-state dispersions in SOC topological insulators (using angle-resolved photoemission spectroscopy, ARPES) (22), or interrogating helical edge state dispersions in real-space photonic crystals (23). Spin-momentum locking is clearly seen in the experimental data (Fig. 2C), as the CW mode transmission predominantly peaks at positive quasimomenta for the lower band. Here we also observe that the direction of spin-momentum locking switches for the upper band.

The Hall ladder exhibits chiral currents – in our system, the CW (CCW) pseudospin evolves preferentially to higher (lower) frequency modes for the lower band. The direction of the current switches for the upper band. To quantify the direction of such spin- and band- dependent frequency evolution we define the steady-state chiral current as

$$j_c = \sum_{m > m_L} P(m, \uparrow) - \sum_{m < m_L} P(m, \uparrow) \quad (4)$$

where m_L is the order of the ring resonance closest to the input laser ($|\omega_{in} - m_L \Omega| < \Omega_R / 2$) and $P(m, \uparrow)$ is the steady-state photon number of the CW mode at frequency $m\Omega$. To measure j_c , we use frequency- and spin-resolved heterodyne detection of the modal photon numbers in the lattice (17). Specifically, we frequency-shift a portion of the input laser by $\delta\omega = 500$ MHz using an acousto-optic modulator and interfere it with the cavity output. Here $\delta\omega \gg |m| \Omega$ for all the modes that we consider. A fast Fourier transform (FFT) of this interferogram directly yields $P(m)$. Heterodyne detection, i.e., the use of a frequency shift as mentioned above, is essential. If one were to set $\delta\omega = 0$ in the experiment described above, one could not distinguish between the photon numbers at $m_L + m$ and $m_L - m$ modes since they produce beat notes at the same radio frequency $m\Omega$. Figure 3A shows the measured chiral current j_c versus the laser detuning $\Delta\omega$. For each $\Delta\omega$, j_c is calculated from the heterodyne FFT spectrum. An example of such a spectrum at $\Delta\omega / K = -0.67$ is shown in Fig. 3B. In Fig. 3C, we show such spectra for all $\Delta\omega$. In Fig. 3D, we show a theoretical computation of the same spectrum. The overall shape of the theoretical spectrum agrees with the experiments. In both the theory and experimental results, in the lower band, the higher frequency modes have a larger occupation ($j_c > 0$). The sign of j_c is switched for the upper band. Alternately, the sign of j_c can be switched by changing the direction of the effective magnetic field (Fig. 3, E and F), which corresponds to exchanging the lengths L_1 and L_2 in our system in Fig. 1A. While our experiments measured the steady-state chiral current, we present theoretical simulations of chiral one-way propagation and the reversal of its direction with a switching of the magnetic flux, in movies S1 to S3 (17). Our simulations show that such one-way propagation is resilient to backscattering around

corners in a finite synthetic lattice for nontrivial fluxes $\phi \neq \pi, 0$, but undergoes strong backreflection for trivial fluxes $\phi = \pi, 0$ (movies S4 and S5) (17).

The Hall ladder in ultracold atomic systems has been predicted to exhibit a phase transition on increasing J/K , from a phase that has a single energy minimum in the ground state (“Meissner” phase) at $k = 0$ to a state that has a pair of energy minima at degenerate k points (“vortex” phase) (19, 24). Here we demonstrate a similar transition in the band structure to illustrate the freedom in our system for shaping photonic bands. We adopt the same terminology to facilitate the comparison with existing literature. In our system, J can be easily tuned by changing the modulation voltage while keeping K constant. For $J/K \ll 1$, the system can be described as a set of decoupled rungs of the ladder. In this regime, the eigenstates are the standing-wave symmetric and antisymmetric supermodes, resulting in flat bands split by $2K$ (Fig. 4, A and E, and inset on the left). Both bands have equal contributions from the CW and CCW legs of the ladder. For $J/K \gg 1$, the two legs of the ladder become decoupled, and we approach the sinusoidal band structure of a 1D-tight binding model with nearest-neighbor coupling (7). In the intermediate regime, the competition between synthetic SOC and effective magnetic field causes a transition in the band structure from a single minimum at $k = 0$ (Fig. 4, A and E) to two minima (Fig. 4, B to H) at (19)

$$k_{g,min} = \pm \arcsin \sqrt{\sin^2 \frac{\phi}{2} - \frac{K^2}{J^2 \tan^2 (\phi/2)}} \quad (5)$$

The experimentally estimated band minima positions agree with the theoretical prediction within measurement uncertainties (Fig. 4J).

By measuring the time-averaged transmission instead of the time-resolved transmission, we detect the spin-projected density of states (DOS) (Fig. 4I). For $J \ll K, \gamma$, two peaks with Lorentzian lineshapes are seen, broadened by the cavity photon decay rate γ (Fig. 4I, blue curve). On increasing J , each of these peaks broadens due to the increasing width of the corresponding band structure (orange curve). Eventually, additional peaks are visible for $J > 2\gamma$ (red and black curves), due to van Hove singularities at the edges of both energy bands (20, 25).

While some aspects such as spin-momentum locking, chiral currents and van Hove singularities have been previously observed in atomic systems (4, 20, 24, 25–29), there are several features that are unique to our photonic implementation. First, we are able to directly measure the dispersion of the chiral one-way modes in synthetic space, thanks to the time-resolved band structure spectroscopy technique, as opposed to mapping of the density-of-states in cold atom experiments (20, 25). Second, we have access to the entire band structure,

including the upper band, which allows us to experimentally observe, for the first time, the chirality switching (Fig. 3) when going from the lower to the upper band in a Hall ladder. Finally, our system exhibits frequency conversion, which can have applications in spectral manipulation of light. For example, the change in the dispersion relations associated with the Meissner-to-vortex phase transition can be used for tunable frequency conversion and frequency comb generation with tailorable spectral envelopes, as shown in fig. S5 (17). All of these features are achieved in a simple photonic structure consisting of a single modulated ring, completely based on the synthetic dimension concept.

Several new possibilities and future applications may be enabled using concepts demonstrated in our experiments. A very interesting possibility is the implementation of interacting Hamiltonians in synthetic frequency dimensions by introducing optical nonlinearities (29, 30), which would permit the study of fundamental many-body physics (31) and have applications in quantum simulation (1) and quantum information processing. Combining with ideas from quantum photonics, one can generate high-dimensional hyperentanglement in pseudospin and frequency axes by exciting the CW and CCW modes with entangled photon pairs (9). Moreover, extensions of our setup can be used to manipulate photonic degrees of freedom, not only limited to frequency conversion but also including topologically protected manipulation of orbital angular momentum (9, 32) and transverse spatial modes (5). The advent of nanophotonic lithium niobate microring modulators with bandwidths exceeding the ring FSR shows promise for realizing synthetic frequency dimensions on chip (33). We anticipate that similar synthetic space concepts could be extended to other frequency ranges such as microwaves (34), or to real-space photonic systems where SOC (35), chiral quantum emission and spin-momentum locking have been reported (36, 37). Additionally, CW-CCW mode excitation in microrings has been explored for studying non-Hermitian physics (38), counterpropagating solitons (39, 40) and topological insulator lasers (41). These ideas can be combined with concepts of gauge potentials, effective magnetic fields and SOC that we have demonstrated here to manipulate and control light in versatile ways.

REFERENCES AND NOTES

- O. Boada, A. Celi, J. I. Latorre, M. Lewenstein, Quantum simulation of an extra dimension. *Phys. Rev. Lett.* **108**, 133001 (2012). [doi:10.1103/PhysRevLett.108.133001](https://doi.org/10.1103/PhysRevLett.108.133001) [Medline](#)
- L. Yuan, Q. Lin, M. Xiao, S. Fan, Synthetic dimension in photonics. *Optica* **5**, 1396–1405 (2018). [doi:10.1364/OPTICA.5.001396](https://doi.org/10.1364/OPTICA.5.001396)
- T. Ozawa, H. M. Price, Topological quantum matter in synthetic dimensions. *Nat. Rev. Phys.* **1**, 349–357 (2019). [doi:10.1038/s42254-019-0045-3](https://doi.org/10.1038/s42254-019-0045-3)
- M. Mancini, G. Pagano, G. Cappellini, L. Livi, M. Rider, J. Catani, C. Sias, P. Zoller, M. Inguscio, M. Dalmonte, L. Fallani, Observation of chiral edge states with neutral fermions in synthetic Hall ribbons. *Science* **349**, 1510–1513 (2015). [doi:10.1126/science.aaa8736](https://doi.org/10.1126/science.aaa8736) [Medline](#)
- E. Lustig, S. Weimann, Y. Plotnik, Y. Lumer, M. A. Bandres, A. Szameit, M. Segev, Photonic topological insulator in synthetic dimensions. *Nature* **567**, 356–360 (2019). [doi:10.1038/s41586-019-0943-7](https://doi.org/10.1038/s41586-019-0943-7) [Medline](#)
- B. A. Bell, K. Wang, A. S. Solntsev, D. N. Neshev, A. A. Sukhorukov, B. J. Eggleton, Spectral photonic lattices with complex long-range coupling. *Optica* **4**, 1433–1436 (2017). [doi:10.1364/OPTICA.4.001433](https://doi.org/10.1364/OPTICA.4.001433)
- A. Dutt, M. Minkov, Q. Lin, L. Yuan, D. A. B. Miller, S. Fan, Experimental band structure spectroscopy along a synthetic dimension. *Nat. Commun.* **10**, 3122 (2019). [doi:10.1038/s41467-019-11117-9](https://doi.org/10.1038/s41467-019-11117-9) [Medline](#)
- A. Regensburger, C. Bersch, M.-A. Miri, G. Onishchukov, D. N. Christodoulides, U. Peschel, Parity-time synthetic photonic lattices. *Nature* **488**, 167–171 (2012). [doi:10.1038/nature11298](https://doi.org/10.1038/nature11298) [Medline](#)
- L. Yuan, Q. Lin, A. Zhang, M. Xiao, X. Chen, S. Fan, Photonic Gauge Potential in One Cavity with Synthetic Frequency and Orbital Angular Momentum Dimensions. *Phys. Rev. Lett.* **122**, 083903 (2019). [doi:10.1103/PhysRevLett.122.083903](https://doi.org/10.1103/PhysRevLett.122.083903) [Medline](#)
- I. Martin, G. Refael, B. Halperin, Topological Frequency Conversion in Strongly Driven Quantum Systems. *Phys. Rev. X* **7**, 041008 (2017). [doi:10.1103/PhysRevX.7.041008](https://doi.org/10.1103/PhysRevX.7.041008)
- M. Lohse, C. Schweizer, H. M. Price, O. Zilberberg, I. Bloch, Exploring 4D quantum Hall physics with a 2D topological charge pump. *Nature* **553**, 55–58 (2018). [doi:10.1038/nature25000](https://doi.org/10.1038/nature25000) [Medline](#)
- O. Zilberberg, S. Huang, J. Guglielmon, M. Wang, K. P. Chen, Y. E. Kraus, M. C. Rechtsman, Photonic topological boundary pumping as a probe of 4D quantum Hall physics. *Nature* **553**, 59–62 (2018). [doi:10.1038/nature25011](https://doi.org/10.1038/nature25011) [Medline](#)
- L. Yuan, Y. Shi, S. Fan, Photonic gauge potential in a system with a synthetic frequency dimension. *Opt. Lett.* **41**, 741–744 (2016). [doi:10.1364/OL.41.000741](https://doi.org/10.1364/OL.41.000741) [Medline](#)
- M. Wimmer, H. M. Price, I. Carusotto, U. Peschel, Experimental measurement of the Berry curvature from anomalous transport. *Nat. Phys.* **13**, 545–550 (2017). [doi:10.1038/nphys4050](https://doi.org/10.1038/nphys4050)
- T. Ozawa, H. M. Price, N. Goldman, O. Zilberberg, I. Carusotto, Synthetic dimensions in integrated photonics: From optical isolation to four-dimensional quantum Hall physics. *Phys. Rev. A* **93**, 043827 (2016). [doi:10.1103/PhysRevA.93.043827](https://doi.org/10.1103/PhysRevA.93.043827)
- C. Qin, F. Zhou, Y. Peng, D. Sounas, X. Zhu, B. Wang, J. Dong, X. Zhang, A. Alù, P. Lu, Spectrum Control through Discrete Frequency Diffraction in the Presence of Photonic Gauge Potentials. *Phys. Rev. Lett.* **120**, 133901 (2018). [doi:10.1103/PhysRevLett.120.133901](https://doi.org/10.1103/PhysRevLett.120.133901) [Medline](#)
- See supplementary materials.
- K. Fang, Z. Yu, S. Fan, Realizing effective magnetic field for photons by controlling the phase of dynamic modulation. *Nat. Photonics* **6**, 782–787 (2012). [doi:10.1038/nphoton.2012.236](https://doi.org/10.1038/nphoton.2012.236)
- D. Hügél, B. Paredes, Chiral ladders and the edges of quantum Hall insulators. *Phys. Rev. A* **89**, 023619 (2014). [doi:10.1103/PhysRevA.89.023619](https://doi.org/10.1103/PhysRevA.89.023619)
- S. Kolkowitz, S. L. Bromley, T. Bothwell, M. L. Wall, G. E. Marti, A. P. Koller, X. Zhang, A. M. Rey, J. Ye, Spin-orbit-coupled fermions in an optical lattice clock. *Nature* **542**, 66–70 (2017). [doi:10.1038/nature20811](https://doi.org/10.1038/nature20811) [Medline](#)
- A. Dutt, M. Minkov, Q. Lin, L. Yuan, D. A. B. Miller, S. Fan, Experimental Demonstration of Dynamical Input Isolation in Nonadiabatically Modulated Photonic Cavities. *ACS Photonics* **6**, 162–169 (2019). [doi:10.1021/acsphotonics.8b01310](https://doi.org/10.1021/acsphotonics.8b01310)
- D. Hsieh, D. Qian, L. Wray, Y. Xia, Y. S. Hor, R. J. Cava, M. Z. Hasan, A topological Dirac insulator in a quantum spin Hall phase. *Nature* **452**, 970–974 (2008). [doi:10.1038/nature06843](https://doi.org/10.1038/nature06843) [Medline](#)
- N. Parappurath, F. Alpeggiani, L. Kuipers, E. Verhagen, Direct Observation of Topological Edge States in Silicon Photonic Crystals: Spin, Dispersion, and Chiral Routing. *arXiv:1811.10739* (2018).
- M. Atala, M. Aidelsburger, M. Lohse, J. T. Barreiro, B. Paredes, I. Bloch, Observation of chiral currents with ultracold atoms in bosonic ladders. *Nat. Phys.* **10**, 588–593 (2014). [doi:10.1038/nphys2998](https://doi.org/10.1038/nphys2998)
- L. F. Livi, G. Cappellini, M. Diem, L. Franchi, C. Clivati, M. Frittelli, F. Levi, D. Calonico, J. Catani, M. Inguscio, L. Fallani, Synthetic Dimensions and Spin-Orbit Coupling with an Optical Clock Transition. *Phys. Rev. Lett.* **117**, 220401 (2016). [doi:10.1103/PhysRevLett.117.220401](https://doi.org/10.1103/PhysRevLett.117.220401) [Medline](#)
- L. W. Cheuk, A. T. Sommer, Z. Hadzibabic, T. Yefsah, W. S. Bakr, M. W. Zwierlein,

- Spin-injection spectroscopy of a spin-orbit coupled Fermi gas. *Phys. Rev. Lett.* **109**, 095302 (2012). [doi:10.1103/PhysRevLett.109.095302](https://doi.org/10.1103/PhysRevLett.109.095302) [Medline](#)
27. F. A. An, E. J. Meier, B. Gadway, Direct observation of chiral currents and magnetic reflection in atomic flux lattices. *Sci. Adv.* **3**, e1602685 (2017). [doi:10.1126/sciadv.1602685](https://doi.org/10.1126/sciadv.1602685) [Medline](#)
 28. H. Cai, J. Liu, J. Wu, Y. He, S.-Y. Zhu, J.-X. Zhang, D.-W. Wang, Experimental Observation of Momentum-Space Chiral Edge Currents in Room-Temperature Atoms. *Phys. Rev. Lett.* **122**, 023601 (2019). [doi:10.1103/PhysRevLett.122.023601](https://doi.org/10.1103/PhysRevLett.122.023601) [Medline](#)
 29. M. E. Tai, A. Lukin, M. Rispoli, R. Schittko, T. Menke, P. M. Dan Borgnia, P. M. Preiss, F. Grusdt, A. M. Kaufman, M. Greiner, Microscopy of the interacting Harper-Hofstadter model in the two-body limit. *Nature* **546**, 519–523 (2017). [doi:10.1038/nature22811](https://doi.org/10.1038/nature22811) [Medline](#)
 30. L. Yuan, A. Dutt, M. Qin, S. Fan, X. Chen, Creating locally interacting Hamiltonians in the synthetic frequency dimension for photons. [arXiv:1909.12466](https://arxiv.org/abs/1909.12466) (2019).
 31. R. Ma, B. Saxberg, C. Owens, N. Leung, Y. Lu, J. Simon, D. I. Schuster, A dissipatively stabilized Mott insulator of photons. *Nature* **566**, 51–57 (2019). [doi:10.1038/s41586-019-0897-9](https://doi.org/10.1038/s41586-019-0897-9) [Medline](#)
 32. X.-W. Luo, X. Zhou, C.-F. Li, J.-S. Xu, G.-C. Guo, Z.-W. Zhou, Quantum simulation of 2D topological physics in a 1D array of optical cavities. *Nat. Commun.* **6**, 7704 (2015). [doi:10.1038/ncomms8704](https://doi.org/10.1038/ncomms8704) [Medline](#)
 33. C. Reimer, Y. Hu, A. Shams-Ansari, M. Zhang, M. Loncar, High-dimensional frequency crystals and quantum walks in electro-optic microcombs. [arXiv:1909.01303](https://arxiv.org/abs/1909.01303) (2019).
 34. C. W. Peterson, W. A. Benalcazar, M. Lin, T. L. Hughes, G. Bahl, Strong Nonreciprocity in Modulated Resonator Chains through Synthetic Electric and Magnetic Fields. *Phys. Rev. Lett.* **123**, 063901 (2019). [doi:10.1103/PhysRevLett.123.063901](https://doi.org/10.1103/PhysRevLett.123.063901) [Medline](#)
 35. D. L. P. Vitullo, C. C. Leary, P. Gregg, R. A. Smith, D. V. Reddy, S. Ramachandran, M. G. Raymer, Observation of Interaction of Spin and Intrinsic Orbital Angular Momentum of Light. *Phys. Rev. Lett.* **118**, 083601 (2017). [doi:10.1103/PhysRevLett.118.083601](https://doi.org/10.1103/PhysRevLett.118.083601) [Medline](#)
 36. S. Barik, A. Karasahin, C. Flower, T. Cai, H. Miyake, W. DeGottardi, M. Hafezi, E. Waks, A topological quantum optics interface. *Science* **359**, 666–668 (2018). [doi:10.1126/science.aar0327](https://doi.org/10.1126/science.aar0327) [Medline](#)
 37. K. Y. Bliokh, D. Smirnova, F. Nori, OPTICS. Quantum spin Hall effect of light. *Science* **348**, 1448–1451 (2015). [doi:10.1126/science.aaa9519](https://doi.org/10.1126/science.aaa9519) [Medline](#)
 38. S. Malzard, H. Schomerus, Bulk and edge-state arcs in non-Hermitian coupled-resonator arrays. *Phys. Rev. A* **98**, 033807 (2018). [doi:10.1103/PhysRevA.98.033807](https://doi.org/10.1103/PhysRevA.98.033807)
 39. Q.-F. Yang, X. Yi, K. Y. Yang, K. Vahala, Counter-propagating solitons in microresonators. *Nat. Photonics* **11**, 560–564 (2017). [doi:10.1038/nphoton.2017.117](https://doi.org/10.1038/nphoton.2017.117)
 40. C. Joshi, A. Klenner, Y. Okawachi, M. Yu, K. Luke, X. Ji, M. Lipson, A. L. Gaeta, Counter-rotating cavity solitons in a silicon nitride microresonator. *Opt. Lett.* **43**, 547–550 (2018). [doi:10.1364/OL.43.000547](https://doi.org/10.1364/OL.43.000547) [Medline](#)
 41. M. A. Bandres, S. Wittek, G. Harari, M. Parto, J. Ren, M. Segev, D. N. Christodoulides, M. Khajavikhan, Topological insulator laser: Experiments. *Science* **359**, eaar4005 (2018). [doi:10.1126/science.aar4005](https://doi.org/10.1126/science.aar4005) [Medline](#)
 42. M. Minkov, S. Fan, Unidirectional light transport in dynamically modulated waveguides. *Phys. Rev. Appl.* **10**, 044028 (2018). [doi:10.1103/PhysRevApplied.10.044028](https://doi.org/10.1103/PhysRevApplied.10.044028)
 43. K. Numata, J. Camp, M. A. Krainak, L. Stolpner, Performance of planar-waveguide external cavity laser for precision measurements. *Opt. Express* **18**, 22781–22788 (2010). [doi:10.1364/OE.18.022781](https://doi.org/10.1364/OE.18.022781) [Medline](#)
 44. M. Hafezi, S. Mittal, J. Fan, A. Migdall, J. M. Taylor, Imaging topological edge states in silicon photonics. *Nat. Photonics* **7**, 1001–1005 (2013). [doi:10.1038/nphoton.2013.274](https://doi.org/10.1038/nphoton.2013.274)

ACKNOWLEDGMENTS

We gratefully acknowledge D.A.B. Miller for initial discussions on the experiment and for providing lab space and equipment. **Funding:** This work is supported by a Vannevar Bush Faculty Fellowship (Grant No. N00014-17-1-3030) from the U. S. Department of Defense, and by MURI grants from the U. S. Air Force Office of Scientific Research (Grant No. FA9550-17-1-0002, FA9550-18-1-0379). L.Y. acknowledges support from the National Natural Science Foundation of China (Grant no. 11974245). M.M. acknowledges support from the Swiss National Science Foundation (Grant No. P300P2_177721). **Author contributions:** Q.L. developed the idea in conjunction with from L.Y. and A.D. A.D. designed, built, and characterized the setup, and collected the data, in consultation with L.Y., Q.L., and S.F. M.M. and Q.L. contributed to theoretical analysis, simulations, and interpretations, with inputs from S.F., M.X. and L.Y. All authors contributed to discussion of the results and writing the manuscript. S.F. supervised the project. **Competing interests:** The authors declare no competing interests. **Data and materials availability:** All data are available in the manuscript or the supplementary materials.

SUPPLEMENTARY MATERIALS

science.sciencemag.org/cgi/content/full/science.aaz3071/DC1

Materials and Methods

Figs. S1 to S5

References (42–44)

Movies S1 to S5

29 August 2019; accepted 13 November 2019

Published online 28 November 2019

10.1126/science.aaz3071

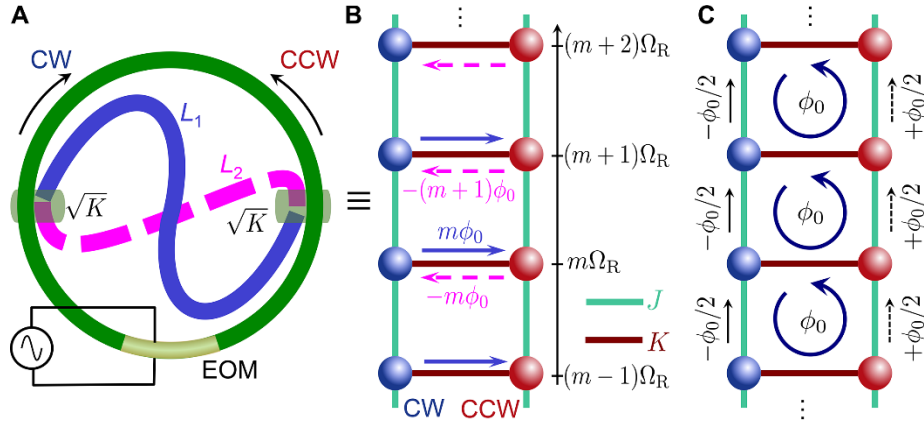


Fig. 1. A modulated ring resonator with clockwise-counterclockwise (CW-CCW) mode-coupling and its corresponding lattice in synthetic dimensions. (A) Schematic of the ring of length L_0 with electro-optic modulation (EOM) and CW-CCW coupling. The CW and CCW modes form the pseudospin degree of freedom. The longitudinal modes of the ring separated by the FSR Ω_R form the frequency degree of freedom. The two directional couplers are connected into an 8-shaped coupler by two connecting waveguides of unequal lengths L_1 and L_2 . By varying $\Delta L = L_1 - L_2$, the phases of couplings between CW and CCW modes [in (B) and (C)] can be varied, hence realizing a controllable effective magnetic field penetrating the ladder. The corresponding synthetic lattice is shown in two equivalent gauges: (B) A gauge with real inter-rung coupling J but complex inter-leg coupling (Eq. 1), (C) a translationally invariant gauge (Eq. 2) with real inter-leg coupling K and complex inter-rung coupling.

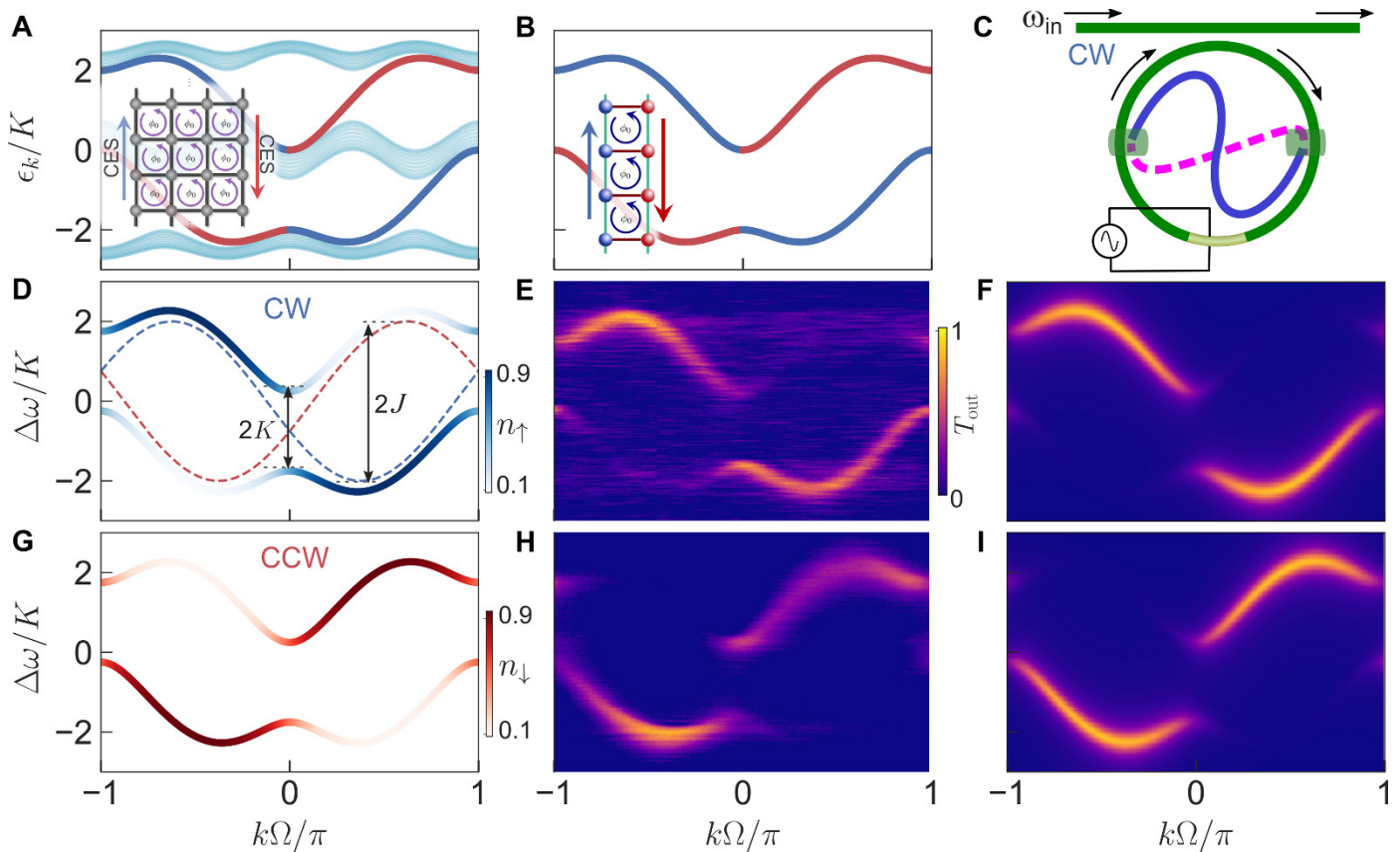


Fig. 2. Chiral band structure and spin-momentum locking in the synthetic Hall ladder. (A) Projected band structure of a 2D quantum Hall insulator infinite along the vertical direction and finite along the horizontal direction (as shown in the inset), showing topological chiral edge states highlighted in blue and red between the bulk band gaps. $\phi = 2\pi/3$. (B) Band structure of the two-legged synthetic Hall ladder from the tight-binding Hamiltonian $\mathcal{H}(k)$ (Eqs. 2 and 3) for $J/K = 2$. The bulk bands disappear but signatures of chiral edge states are preserved (19). (C) Schematic setup to directly measure band structure by coupling an input-output waveguide to the ring in Fig. 1A. By varying ω_{in} and detecting the time-resolved transmission through the ring, the band structure can be directly read out in experiments. The CW (CCW)-spin-resolved band structure can be detected by exciting the waveguide from the left (right) and recording its transmission. (D and G) Theoretical band structures, with color-coded pseudospin projections n_{\uparrow} and n_{\downarrow} for corresponding eigenstates. For the lower band, $+k$ states have predominantly CW pseudospin character, signifying spin-momentum locking. The dashed lines are band structures for the same J but for $K = 0$. (E and H) Experimental time-resolved transmission through the ring for CW excitation (E) and CCW excitation (H). $\Delta\omega$ is the detuning of the input frequency ω_{in} from the resonance frequency of the uncoupled CW and CCW modes. (F and I) Theoretical time-resolved transmission based on Floquet analysis (see supplementary materials). Experimental parameters: $J/2\pi = 1.95$ MHz, $K/2\pi = 0.97$ MHz. $\phi \approx 3\pi/4$. Cavity linewidth $\gamma/2\pi = 480$ kHz.

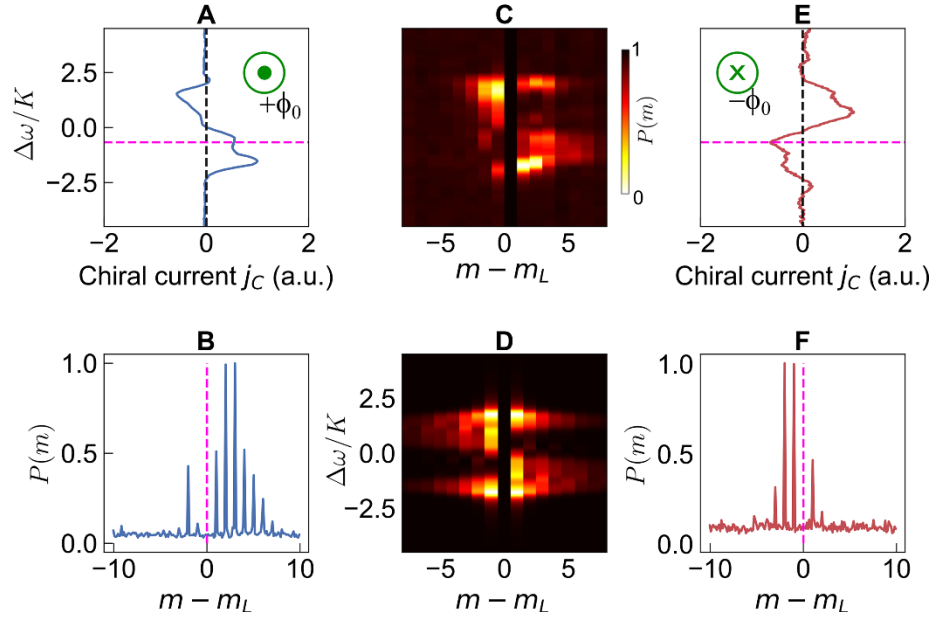


Fig. 3. Direct measurements of chiral currents in the synthetic Hall ladder through heterodyne detection. (A) Chiral current j_C (Eq. 4) vs. laser-cavity detuning $\Delta\omega$ measured by heterodyne mixing the cavity output field with a frequency shifted part of the input laser. The full heterodyne signal is shown in (E). The lower band shows a positive j_C for the CW mode. (B) Steady state normalized photon number of the modes at frequencies $m\Omega$ in the lower band, at $\Delta\omega/K = -0.67$ indicated by the magenta dashed line in (A). The asymmetric frequency mode occupation verifies that the CW mode predominantly evolves toward higher frequencies in the lower band. (C) Experimental heterodyne spectra mapping out the steady state photon numbers for all $\Delta\omega$. (D) Theoretically calculated photon numbers based on a Floquet analysis. (E and F) Same as in (A) and (B), but with the direction of the effective magnetic field flipped, which causes a change in the sign of j_C . (A) and (C) also reveal a switching of the direction of chiral current on moving from the lower to the upper band. In (C) and (D), the strong signal in the excited mode ($m - m_L = 0$) has been suppressed to reveal the occupation of other modes clearly.

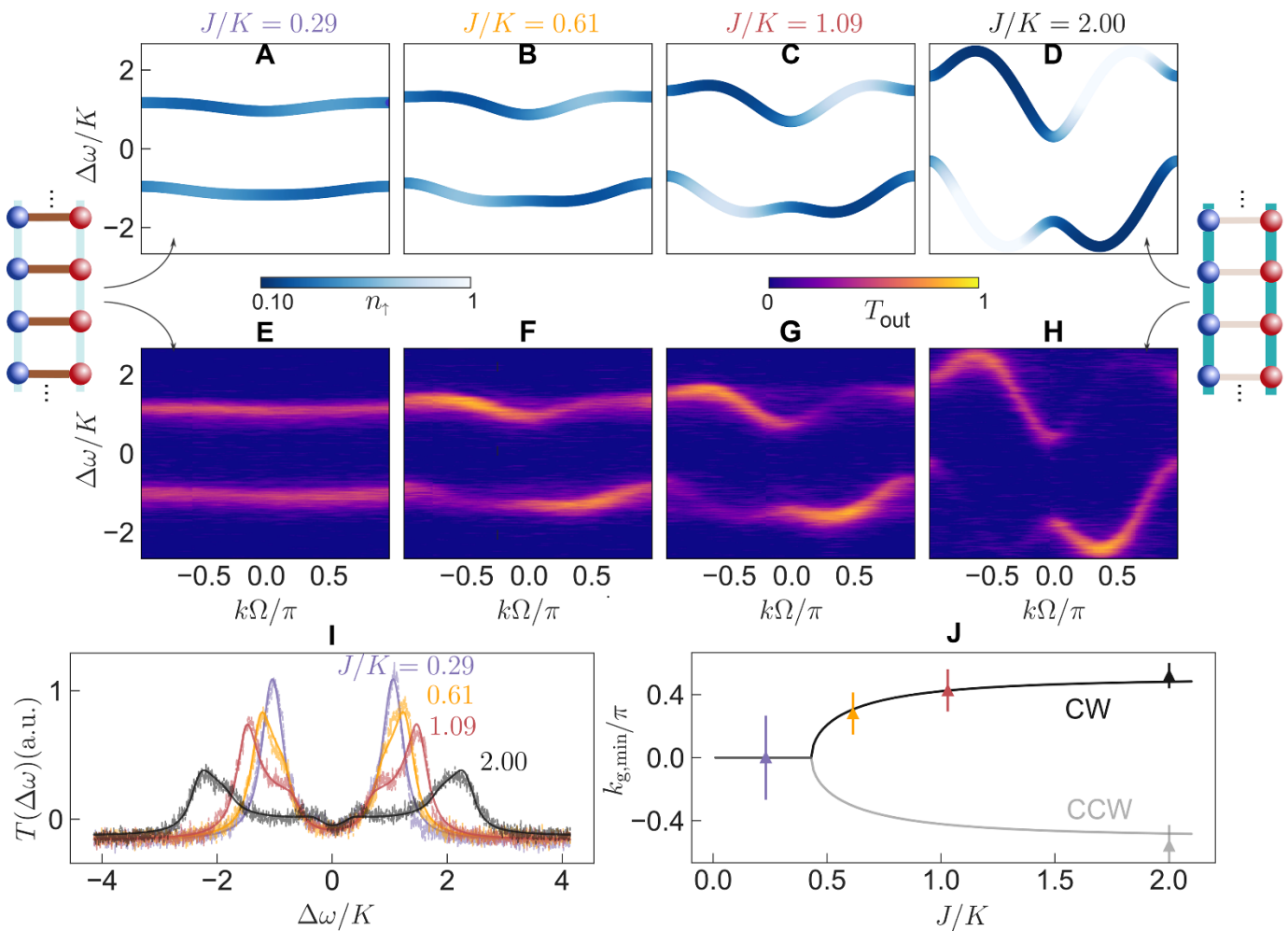


Fig. 4. Observation of phase transition through spin-resolved band structure measurements. Top row (A to D) Theoretical band structure for $\phi_0 = 2.38 \approx 3\pi/4$, for increasing J/K . Middle row (E to H) Corresponding experimentally measured time-resolved transmission showing good agreement with theory. The ladder insets in the left and right are indicative of the strengths in the pseudospin and frequency axes. J can be continuously tuned by varying the amplitude of the modulation signal. (I) Time-averaged transmission revealing the density of states (DOS). Van Hove singularities due to a diverging DOS are also visible in the transmission, smeared out by the cavity decay rate $\gamma/K = 0.37$. (J) Bifurcation of the energy minimum in k . Data points represent experimentally estimated splittings for band structures shown in the middle row, which agree with the solid lines based on Eq. 5.

A single photonic cavity with two independent physical synthetic dimensions

Avik Dutt, Qian Lin, Luqi Yuan, Momchil Minkov, Meng Xiao and Shanhui Fan

published online November 28, 2019 originally published online November 28, 2019

ARTICLE TOOLS

<http://science.sciencemag.org/content/early/2019/12/02/science.aaz3071>

SUPPLEMENTARY MATERIALS

<http://science.sciencemag.org/content/suppl/2019/11/25/science.aaz3071.DC1>

REFERENCES

This article cites 44 articles, 5 of which you can access for free
<http://science.sciencemag.org/content/early/2019/12/02/science.aaz3071#BIBL>

PERMISSIONS

<http://www.sciencemag.org/help/reprints-and-permissions>

Use of this article is subject to the [Terms of Service](#)

Science (print ISSN 0036-8075; online ISSN 1095-9203) is published by the American Association for the Advancement of Science, 1200 New York Avenue NW, Washington, DC 20005. The title *Science* is a registered trademark of AAAS.

Copyright © 2019, American Association for the Advancement of Science